

# MHD Free Convection in an Enclosure Loaded with Nanofluid and Partially Cross-heated

A. Marfouk<sup>1</sup>, A. Mansour<sup>2†</sup>, A. Hasnaoui<sup>1</sup>, A. Amahmid<sup>2</sup> and M. Hasnaoui<sup>2</sup>

<sup>1</sup> LS3M Laboratory, Polydisciplinary Faculty of Khouribga, Sultan Moulay Slimane University, 25000 Khouribga, Morocco

<sup>2</sup> Cadi Ayyad University, Faculty of Sciences Semlalia, Department of Physics, LMFE, BP 2390 Marrakesh, Morocco

†Corresponding Author Email: [a.mansour@uca.ac.ma](mailto:a.mansour@uca.ac.ma)

## ABSTRACT

This paper digitally examines natural convection in a porous cavity laden with nanofluids. The influence of Brownian motion and thermophoresis on particle motion through the Buongiorno model is reviewed. The application of the Darcy-Brinkman model makes it possible to simulate the transfer of momentum under the effect of a horizontal magnetic field. Two segments located in the central parts of the left and bottom walls heat the cavity. The right wall is cooled at a constant temperature and the remaining surfaces of the cavity boundary are insulated. A computational code, designed on the principles of the finite volume method in conjunction with the SIMPLE algorithm, is employed to address the fundamental equations governing the system effectively. The numerical results are illustrated by presenting streamlines, isotherms, iso-concentrations and local and mean Nusselt numbers. The dimensionless parameters that change are the Rayleigh number ( $10^3 \leq R_T \leq 10^6$ ), the Darcy number ( $10^{-5} \leq Da \leq 10^{-2}$ ), the Hartmann number ( $0 \leq Ha \leq 100$ ), the thermophoresis parameter ( $0.05 \leq N_t \leq 0.5$ ), the Brownian motion parameter ( $0.05 \leq N_b \leq 0.5$ ), and the buoyancy parameter ( $0.05 \leq N_r \leq 0.5$ ). The increase in  $R_T$  leads to an improvement in the heat transfer rate and an attenuation of the inhomogeneity of the distribution of nanoparticles in the cavity. A reverse tendency is observed by increasing the intensity of the magnetic field. Moreover, the parameters  $N_t$  and  $N_b$  exhibit a more significant impact on the Sherwood number than on the Nusselt number.

## Article History

Received October 1, 2024

Revised February 7, 2025

Accepted February 17, 2025

Available online May 5, 2025

## Keywords:

Magnetic field

Square cavity

Finite volume method

Heat mass transfer

Buongiorno model

## 1. INTRODUCTION

Natural convection induced by magnetohydrodynamics (MHD) in porous media is receiving growing attention due to its importance in various applications. These applications include high-performance insulation for buildings, solar collectors, cooling of electronic devices, and nuclear reactors (see, for example, [Bondareva et al., 2016, 2017](#); [Alsabery et al., 2018](#); [Ahmed et al., 2020](#)). Conventional working fluids, such as water and oils with low thermal conductivity, have been used for a long time. However, their low conductivity poses a barrier to improving the thermal efficiency of many engineering systems. Dispersing solid particles of nanometric sizes (from 10 to 100 nm) in the base fluid significantly enhances heat transfer. [Choi and Eastman \(1995\)](#) first introduced the term of nanofluid to describe a fluid containing suspended highly conductive solid metal particles. Researchers worldwide have explored various

geometrical configurations using different types of nanofluids. Their results generally confirm an improvement in heat transfer compared to conventional base fluids ([Kahveci, 2010](#); [Kasaeian et al., 2017](#); [Babar & Ali, 2019](#); [Khanafar & Vafai, 2019](#); [Rahimi et al., 2019](#); [Nazari, 2019](#)). The authors have explored the interaction between nanofluids and magnetic fields in many studies ([Nazari et al., 2019](#); [Prakash et al., 2019a,b](#); [Narla et al., 2020](#); [Prakash et al., 2020](#)).

[Sheikholeslami and Ellahi \(2015\)](#) investigated the hydrothermal treatment of a magnetohydrodynamic nanofluid contained within a cubic cavity that was heated from below. In this study, the magnetic field induces a slowdown in fluid flow, consequently reducing the impact of convection. In addition, the Nusselt number increases with rising Rayleigh numbers and higher nanofluid volume fractions. Conversely, an increase in the intensity of the magnetic field results in a reduction of the Nusselt number.

NOMENCLATURE			
$B_0$	magnitude of external magnetic field	$u, v$	velocity components in the $x$ - and $y$ -directions
$Da$	Darcy number	$U, V$	dimensionless velocity components in the $x$ -direction and $y$ -direction
$D_B$	Brownian diffusion coefficient	$x, y$ & $X, Y$	space coordinates & dimensionless space coordinates
$D_T$	thermophoretic diffusion coefficient	$\alpha$	thermal diffusivity
$g$	gravitational acceleration	$\beta$	thermal expansion coefficient
$h$	length of partially heated wall	$\varepsilon$	porosity
$Ha$	Hartmann number	$\mu$	dynamic viscosity
$k$	thermal conductivity	$\tau$	dimensionless time
$K$	permeability	$\rho$	density
$L$	length of enclosure	$\Psi$	stream function
$Le$	Lewis number	$\theta$	dimensionless temperature
$MHD$	magnetohydrodynamic	$\phi$	dimensionless solid volume fraction
$N_b$	Brownian motion parameter	$\varphi$	nanoparticles volume fraction
$N_r$	buoyancy ratio parameter	$\varphi_0$	reference nanoparticles volume fraction
$N_t$	thermophoresis parameter	$\sigma$	electrical conductivity
$Nu$	local Nusselt number	<b>Subscripts</b>	
$Nu_{avg}$	average Nusselt number	$avg$	average
$p$	dimensional pressure	$b$	bottom
$P$	non-dimensional pressure	$c$	cold
$Pr$	Prandtl number	$f$	fluid
$R_T$	Rayleigh number	$h$	hot
$Sh$	local Sherwood number	$l$	left
$Sh_{avg}$	average Sherwood number	$nf$	nanofluid
$t$	dimensional time	$p$	porous
$T$	dimensional temperature	$s$	solid particles

[Sheikholeslami \(2018a\)](#) investigated the effects of an imposed magnetic field on the radiative and convective heat transfer of ferrofluid in a cavity containing a circular hot cylinder. The findings indicate that an increase in the radiation parameter and the Rayleigh number intensifies the temperature gradients. Conversely, an increase in Lorentz forces leads to a reduction in temperature gradients.

[Li et al. \(2024a\)](#) examined the heat and mass transfer characteristics of two types of nanofluids flowing around a solid sphere. Their study specifically investigated the coupled effects of linear thermal radiation and chemical reactions on these transfer phenomena.

Mixed convective Darcy–Forchheimer flow of nanofluid is studied in the presence of viscous dissipation effects.

[Li et al. \(2024b\)](#) studied the mixed convection of a nanofluid within a porous cavity using the Darcy–Forchheimer model. They incorporating it the effects of viscous dissipation. The results indicate that increased Brinkman numbers, which correspond to higher permeability, enhance heat transfer rates. Additionally, the concentration of nanofluid rises with an increase of the Soret number. The study further reveals that wall shear forces exhibit a positive correlation with the Hartmann number and the variable thermal conductivity coefficient. [Buongiorno \(2006\)](#) identified Brownian diffusion and thermophoresis as fundamental mechanisms governing slip in nanofluids and developed a transport model incorporating these effects. [Kefayati \(2014\)](#) investigated

the combined influence of nanoparticle volume fraction, Rayleigh number, and magnetic field on heat transfer within a cavity featuring a linearly heated wall. [Oztop and Abu-Nada \(2008\)](#) conducted a numerical study on free convection driven by buoyancy forces in an enclosure partially heated and filled with nanofluids containing different types of nanoparticles. Their findings highlighted that heat transfer enhancement is more pronounced at lower aspect ratios of the enclosure.

[Benyazer et al. \(2022\)](#) studied natural convection in a porous square cavity filled with nanofluids using Buongiorno's model. The convective heat exchange is affected by the incorporation of nanoscale particles into the base fluid. [Zahmatkesh and Habibi \(2019\)](#) employed the same mathematical framework to examine free and mixed convection in nanofluid-saturated porous square cavities. They analysed the effects of the buoyancy ratio, the thermophoresis number and the Brownian diffusion parameter on flow intensity and mean Nusselt number. The impact of these parameters on the development of streamlines, isotherms and iso-concentrations was also examined. Their results indicated that the thermophoresis number exerts a stronger influence on flow strength and mean Nusselt number than the parameters of Brownian diffusion and buoyancy ratio.

[Sheremet et al. \(2015\)](#) investigated numerically free convection in a right-angle trapezoidal porous cavity loaded with a nanofluid. The thermophoresis and Brownian motion parameters are specifically examined. They revealed that the Nusselt and Sherwood numbers, along with the flow strength, increase with the Rayleigh

number while decreasing with both the aspect ratio and the Lewis number. In addition, the flow strength was hampered by the increase in the buoyancy ratio and the Brownian motion parameter.

Sammoud and Gueraoui (2021) investigated the phenomenon of magnetohydrodynamic (MHD) double-diffusive natural convection in an annular porous medium confined between two concentric vertical cylinders filled with an Al<sub>2</sub>O<sub>3</sub>-water nanofluid. The system underwent a localized heat flux applied to the inner cylinder. The results showed that as the volume fraction of solid nanoparticles increased, the amount of thermal energy transferred also increased. However, the mass transfer at the active wall decreased. In addition, mass and thermal energy transfer rates at the active wall decline with increasing magnetic field intensity.

Sheikholeslami and Shehzad (2017) used the Lattice Boltzmann Method to study the impacts of Rayleigh number and Lorentz force on the non-Darcian convective flow of a nanofluid. This flow adheres to the KKL model within a porous cavity. Their findings indicated that an increase in the Lorentz force leads to a reduction in convective heat transfer. This attenuation of convection due to rising Lorentz forces was further substantiated in their study.

Sheikholeslami (2018b) examined how magnetic forces affect the application of the second law of thermodynamics to ferrofluids. They showed that a decrease in the intensity of these magnetic forces leads to reduced energy losses. Nevertheless, the reduction in magnetic forces provokes a rise in entropy generation within the porous medium. Additionally, enhancing the conduction mode may result in a higher Bejan number.

Sheikholeslami (2019) examined the effects of magnetic forces on magnetohydrodynamic (MHD) convective flow of a nanofluid in a permeable medium. He focused on the effects of the Hartmann and Rayleigh numbers, such as the radiation parameter. The study showed that stronger magnetic forces diminish convection. Additionally, higher radiation intensity lowers the temperature gradient in the fluid.

Motlagh et al. (2016) investigated the influence of porosity, nanoparticle characteristics, and cavity inclination angle on the distribution of nanoparticles. They examined how these factors influence heat transfer due to natural convection in a square porous enclosure filled with a nanofluid. The study employed Buongiorno's two-component model, revealing that porosity significantly influences the heat transfer rate, particularly at elevated porous Rayleigh numbers. Additionally, the study revealed that copper (Cu) nanoparticles exhibit a more uniform distribution within the enclosure than aluminum oxide (Al<sub>2</sub>O<sub>3</sub>) nanoparticles.

Alsabery et al. (2016) employed the finite element method to investigate Darcian natural convection within a partially filled inclined square cavity. The cavity consists of a central square fluid-filled hole surrounded by a nanofluid-saturated porous medium. Their findings demonstrated that the presence of the hole significantly suppresses convective flow. Furthermore, they observed

that the thermal properties and size of the insert exert opposing influences on the convection process.

Jafari et al. (2018) identified the optimal configuration of cylinders to maximise heat transfer efficiency within a porous medium. Their study also provided a comprehensive analysis of the effects of the porous medium on both the flow field and the heat transfer characteristics of nanofluid natural convection.

The influence of a magnetic field on natural convection in a discretely heated square porous cavity filled with nanofluid is not well understood. In this setup, heaters are positioned at the center of the left and bottom walls. Therefore, the present numerical study aims to analyse magnetohydrodynamic (MHD) natural convection of nanofluids in a porous square cavity subjected to partial cross-heating, utilising Buongiorno's mathematical model. This study aims to clarify the fundamental flow physics and evaluate the impact of key controlling parameters. It examines the effects of several dimensionless numbers, including the Rayleigh number, Darcy number, Hartmann number, Brownian motion parameter, thermophoresis parameter, and buoyancy ratio, on fluid flow and heat transfer.

The results of this study could enhance thermal performance and improve heat transfer in various engineering applications, especially in electronic cooling systems. The numerical code has been rigorously validated against previous studies, and the results are presented and analysed in the subsequent sections.

## 2. MATHEMATICAL FORMULATION

The configuration under study is depicted in Fig. 1. It consists of a square porous cavity of height  $L$ , saturated with a nanofluid and partially heated along the central sections of its bottom and left walls. The cavity is cooled from the right wall, while its remaining walls are insulated. The heating and cooling surfaces are maintained at constant temperatures  $T_h$  and  $T_c$ , respectively. The length of heating elements is  $h = \frac{L}{3}$ . This study is conducted for a fixed Lewis number ( $Le = 25$ ) and Prandtl number ( $Pr = 7$ ). The flow is assumed to be 2D and laminar. The effects of Brownian motion and thermophoresis within the nanofluid are considered using the Buongiorno model (2006). Based on these assumptions and using the Boussinesq approximation, the continuity, momentum, energy and nanoparticle transport equations are expressed as follows:

Continuity equation:

$$\frac{\partial u}{\partial x} + \frac{\partial v}{\partial y} = 0 \quad (1)$$

x-momentum equation:

$$\frac{\rho_{nf}}{\varepsilon} \frac{\partial u}{\partial t} + \frac{1}{\varepsilon^2} \left( u \frac{\partial u}{\partial x} + v \frac{\partial u}{\partial y} \right) = -\frac{\partial p}{\partial x} - \frac{\mu_{nf}}{K} u + \frac{\mu_{nf}}{\varepsilon} \left( \frac{\partial^2 u}{\partial x^2} + \frac{\partial^2 u}{\partial y^2} \right) \quad (2)$$

y-momentum equation:

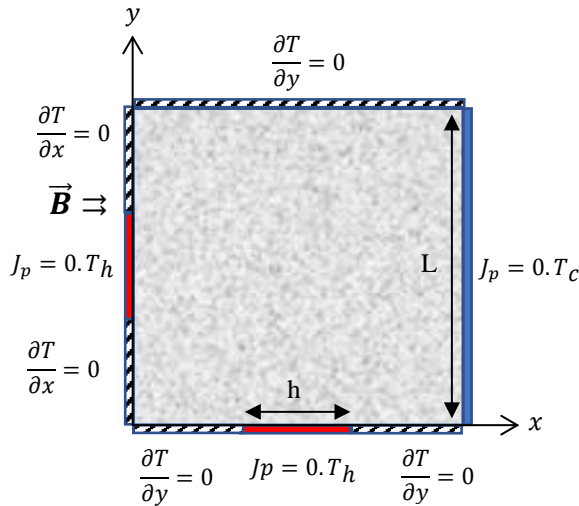


**Fig. 1 Physical problem**

$$\frac{\rho_{nf}}{\varepsilon} \frac{\partial v}{\partial t} + \frac{1}{\varepsilon^2} \left( u \frac{\partial v}{\partial x} + v \frac{\partial v}{\partial y} \right) = -\frac{\partial p}{\partial y} - \frac{\mu_{nf}}{K} v + \frac{\mu_{nf}}{\varepsilon} \left( \frac{\partial^2 v}{\partial x^2} + \frac{\partial^2 v}{\partial y^2} \right) + \left( (1 - \varphi_0) \beta_T \rho_{nf} (T - T_c) + (\rho_p - \rho_{nf}) \varphi \right) g - \sigma_{nf} B_0^2 v \quad (3)$$

Energy equation:

$$\frac{(\rho c)_m}{(\rho c)_{nf}} \frac{\partial T}{\partial t} + \left( u \frac{\partial T}{\partial x} + v \frac{\partial T}{\partial y} \right) = \frac{k_m}{(\rho c)_{nf}} \nabla^2 T + \frac{\varepsilon(\rho c)_p}{(\rho c)_{nf}} \left[ D_B \left( \frac{\partial \varphi}{\partial x} \frac{\partial T}{\partial x} + \frac{\partial \varphi}{\partial y} \frac{\partial T}{\partial y} \right) + \frac{D_T}{T_c} \left( \left( \frac{\partial T}{\partial x} \right)^2 + \left( \frac{\partial T}{\partial y} \right)^2 \right) \right] \quad (4)$$

Nanoparticles volume fraction equation:

$$\frac{\partial \varphi}{\partial t} + \frac{1}{\varepsilon} \left( u \frac{\partial \varphi}{\partial x} + v \frac{\partial \varphi}{\partial y} \right) = D_B \left( \frac{\partial^2 \varphi}{\partial x^2} + \frac{\partial^2 \varphi}{\partial y^2} \right) + \frac{D_T}{T_c} \left( \frac{\partial^2 T}{\partial x^2} + \frac{\partial^2 T}{\partial y^2} \right) \quad (5)$$

Where  $D_B = \frac{k_B T_0}{3\pi d_p \mu_f}$  is the Brownian diffusion coefficient ( $m^2 s^{-1}$ ) and  $D_T = \frac{\zeta \mu C_0}{\rho_f}$  is the thermophoresis diffusion coefficient ( $m^2 s^{-1}$ ). The proportionality factor is given by [McNab and Meisen \(1973\)](#):

$$\zeta = 0.26 \frac{k_f}{k_f + k_p}$$

By introducing the following dimensionless variables:

$$\tau = \frac{\alpha_{nf} t}{L^2}, \quad X = \frac{x}{L}, \quad Y = \frac{y}{L}, \quad U = \frac{uL}{\alpha_{nf}}, \quad V = \frac{vL}{\alpha_{nf}}, \quad \theta = \frac{T - T_c}{T_h - T_c}, \quad \phi = \frac{\varphi}{\varphi_0}, \quad P = \frac{pL^2}{\rho_{nf} \alpha_{nf}}, \quad (6)$$

The previous dimensional equations become:

$$\frac{\partial U}{\partial \tau} + \frac{\partial V}{\partial Y} = 0 \quad (7)$$

$$\varepsilon \frac{\partial U}{\partial \tau} + U \frac{\partial U}{\partial X} + V \frac{\partial U}{\partial Y} = -\varepsilon^2 \frac{\partial P}{\partial X} + \varepsilon Pr \left( \frac{\partial^2 U}{\partial X^2} + \frac{\partial^2 U}{\partial Y^2} \right) - \varepsilon^2 \frac{Pr}{Da} U \quad (8)$$

$$\varepsilon \frac{\partial V}{\partial \tau} + U \frac{\partial V}{\partial X} + V \frac{\partial V}{\partial Y} = -\varepsilon^2 \frac{\partial P}{\partial Y} + \varepsilon Pr \left( \frac{\partial^2 V}{\partial X^2} + \frac{\partial^2 V}{\partial Y^2} \right) - \varepsilon^2 \frac{Pr}{Da} V - \varepsilon^2 Pr Ha^2 V + \varepsilon^2 Pr R_T (\theta - N_r \phi) \quad (9)$$

$$\eta \frac{\partial \theta}{\partial \tau} + U \frac{\partial \theta}{\partial X} + V \frac{\partial \theta}{\partial Y} = \frac{\partial^2 \theta}{\partial X^2} + \frac{\partial^2 \theta}{\partial Y^2} + N_b \left( \frac{\partial \theta}{\partial X} \frac{\partial \phi}{\partial X} + \frac{\partial \theta}{\partial Y} \frac{\partial \phi}{\partial Y} \right) + N_t \left[ \left( \frac{\partial \theta}{\partial X} \right)^2 + \left( \frac{\partial \theta}{\partial Y} \right)^2 \right] \quad (10)$$

$$\varepsilon \frac{\partial \phi}{\partial \tau} + U \frac{\partial \phi}{\partial X} + V \frac{\partial \phi}{\partial Y} = \frac{1}{Le} \left( \frac{\partial^2 \phi}{\partial X^2} + \frac{\partial^2 \phi}{\partial Y^2} \right) + \frac{N_t}{Le N_b} \left( \frac{\partial^2 \theta}{\partial X^2} + \frac{\partial^2 \theta}{\partial Y^2} \right) \quad (11)$$

The dimensionless parameters present in the equations above include the Lewis number ( $Le$ ), the Prandtl number ( $Pr$ ), the Darcy number ( $Da$ ), the Rayleigh number ( $R_T$ ), the Hartmann number ( $Ha$ ), the buoyancy ratio parameter ( $N_r$ ), the parameter of Brownian motion ( $N_b$ ) and the parameter of thermophoresis ( $N_t$ ). They are defined as follows:

$$Le = \frac{\alpha_{nf}}{\varepsilon D_B}, \quad Pr = \frac{\vartheta_{nf}}{\alpha_{nf}}, \quad Da = \frac{K}{L^2}, \quad R_T = \frac{(1 - \varphi_0) \beta_T g (T_h - T_c) L^3}{\vartheta_{nf} \alpha_{nf}}, \quad Ha = \sqrt{\frac{L^2 B_0^2 \sigma}{\mu_{nf}}}, \quad N_r = \frac{(\rho_p - \rho_f) \varphi_0}{(1 - \varphi_0) \beta_T \rho_{nf} (T_h - T_c)}, \quad N_b = \frac{\varphi_0 D_B \varepsilon (\rho C p)_p}{\alpha_{nf} (\rho C p)_{nf}}, \quad N_t = \frac{D_T \varepsilon (\rho C p)_p (T_h - T_c)}{T_c (\rho C p)_{nf} \alpha_{nf}} \quad (12)$$

The boundary conditions are defined as follows:

$$U = 0; V = 0; \theta = 1; J_p = N_t \frac{\partial \theta}{\partial X} + N_b \frac{\partial \phi}{\partial X} = 0 \quad \text{for } (X = 0; \frac{h}{L} \leq Y \leq 1 - \frac{h}{L})$$

$$U = 0; V = 0; \frac{\partial \theta}{\partial X} = 0; \frac{\partial \phi}{\partial X} = 0 \quad \text{for } (X = 0; 0 \leq Y \leq \frac{h}{L})$$

$$U = 0; V = 0; \frac{\partial \theta}{\partial X} = 0; \frac{\partial \phi}{\partial X} = 0 \quad \text{for } (X = 0; 1 - \frac{h}{L} \leq Y \leq 1)$$

$$U = 0; V = 0; \theta = 0; J_p = N_t \frac{\partial \theta}{\partial X} + N_b \frac{\partial \phi}{\partial X} = 0 \quad \text{for } (X = 1; 0 \leq Y \leq 1)$$

$$U = 0; V = 0; \theta = 1; J_p = N_t \frac{\partial \theta}{\partial X} + N_b \frac{\partial \phi}{\partial X} = 0 \quad \text{for } (Y = 0; \frac{h}{L} \leq X \leq 1 - \frac{h}{L})$$

$$U = 0; V = 0; \frac{\partial \theta}{\partial Y} = 0; \frac{\partial \phi}{\partial Y} = 0 \quad \text{for } (Y = 0; 0 \leq X \leq \frac{h}{L})$$

$$U = 0; V = 0; \frac{\partial \theta}{\partial Y} = 0; \frac{\partial \phi}{\partial Y} = 0 \quad \text{for } (Y = 0; 1 - \frac{h}{L} \leq X \leq 1)$$

$$U = 0; V = 0; \frac{\partial \theta}{\partial Y} = 0; \frac{\partial \phi}{\partial Y} = 0 \quad \text{for } (Y = 1; 0 \leq X \leq 1) \quad (13)$$

The local and average Nusselt and Sherwood numbers are defined as:

$$Nu_l = - \left( \frac{\partial \theta}{\partial X} \right)_{X=0} \quad \text{on the vertical heater} \quad (14)$$

$$Nu_b = - \left( \frac{\partial \theta}{\partial Y} \right)_{Y=0} \quad \text{on the horizontal heater} \quad (14)$$

$$Sh_l = - \left( \frac{\partial \phi}{\partial X} \right)_{X=0} \quad \text{on the vertical heater} \quad (15)$$

$$Sh_b = - \left( \frac{\partial \phi}{\partial Y} \right)_{Y=0} \quad \text{on the horizontal heater} \quad (15)$$

$$Nu_{avl} = \frac{1}{h'} \int_a^b Nu_l dy; \quad Nu_{avb} = \frac{1}{h'} \int_a^b Nu_b dx \quad (16)$$

**Table 1 Comparison between our results and those of Shermet et al. (2014) for  $R_T = 100$ ,  $Ha = 0$  and  $N_t = N_b = 0.4$**

$Le$	$N_r$	$Nu_{avg}$		
		Shermet et al. (2014)	Our code	relative deviation
1	0.1	3.8387	3.8178	0.54%
	0.4	2.7791	2.7717	0.27%
10	0.1	4.6270	4.5926	0.74%
	0.4	4.0088	4.0061	0.07%
100	0.1	4.6252	4.5562	1.49%
	0.4	4.3049	4.3387	0.8%

$$Sh_{avl} = \frac{1}{h'} \int_a^b Sh_l dy; Sh_{avb} = \frac{1}{h'} \int_a^b Sh_b dx \quad (17)$$

With  $= \frac{h}{L}$ ,  $b = 1 - \frac{h}{L}$  and  $h' = \frac{h}{L}$

$$Nu_{avg} = \frac{(Nu_{avl} + Nu_{avb})}{2}; Sh_{avg} = \frac{(Sh_{avl} + Sh_{avb})}{2} \quad (18)$$

In this study, attention will be focused on the Nusselt and Sherwood numbers when  $N_t \neq N_b$  and the analysis will be restricted to the Nusselt number when  $N_t = N_b = 0.1$ .

### 3. NUMERICAL METHOD

The governing equations numbered (7) to (11), are solved using the finite volume method in conjunction with the SIMPLE algorithm (Patankar (1980)). Convergence of the calculations is deemed achieved when the following condition was met:

$$Err_W = \frac{\sum_x \sum_y |W_{x,y}^{n+1} - W_{x,y}^n|}{\sum_x \sum_y |W_{x,y}^{n+1}|} < 10^{-6}$$

Where  $W$  stands for  $U$ ,  $V$ ,  $\theta$  and  $\Phi$  and the superscripts  $n$  and  $n + 1$  designate two successive iterations.

Validation of the present code against existing literature is crucial to confirm its accuracy and efficiency. This quantitative validation is performed by comparing our findings with those of Shermet et al. (2014), as demonstrated in Table 1.

The present code reproduces the results of the latter reference with deviations of less than 1.5%. The initial qualitative validation is conducted using the numerical results (streamlines, isotherms, and iso-concentrations) from Zahmatkesh and Habibi (2019). Their study focuses on the natural convection of a nanofluid within a square porous cavity, with constant-temperature side walls (see Fig. 2). The second validation utilises experimental and numerical isotherms plots produced by Calcagni et al. (2005) in a square cavity that is heated from the bottom (see Fig. 3). The qualitative comparisons illustrated in Figs. 2 and 3 further substantiate the reliability of this study numerical code.

A grid sensitivity analysis was conducted using various mesh sizes to determine the most suitable grid for the calculations  $R_T = 10^6$ ,  $Le = 25$ ,  $Da = 10^{-2}$ ,  $Pr = 7$ ,  $N_r = N_t = N_b = 0.1$  and  $Ha = 0$  (see Table 2). The results indicate that the Nusselt number calculated with a

$120 \times 120$  mesh differs by about 0.93% from that obtained with the finest mesh of  $180 \times 180$ . Accordingly, the  $120 \times 120$  grid was considered appropriate for this study.

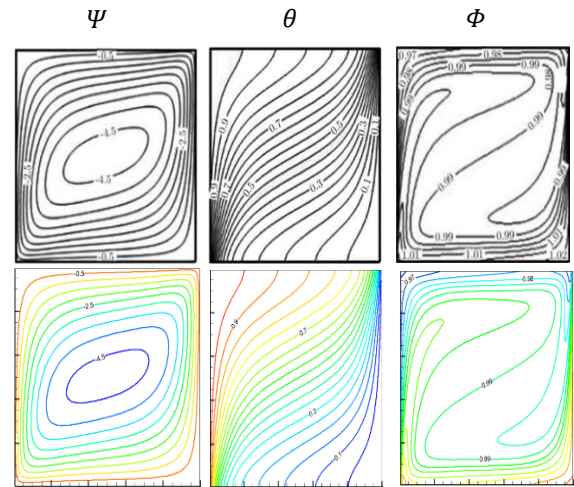


**Fig. 2 Comparison between our results and those of Zahmatkesh and Habibi (2019) in terms of streamlines, isotherms and isocentrations for,  $R_T = 100$ ,  $Ha = 0$ ,  $N_t = 0.05$ , and  $N_b = N_r = 0.1$**

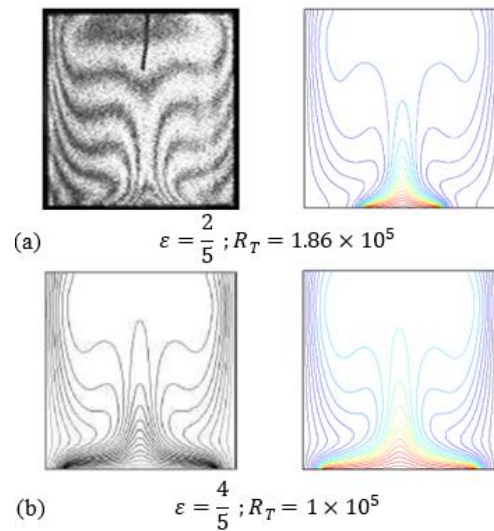


**Fig. 3 Validation in terms of isotherms (right side) and those of Calcagni et al. (2005): experimental (a) and numerical (b) results**

**Table 2 Effect of the grid size on the average Nusselt number for  $R_T = 10^6$ ,  $Da = 10^{-2}$ ,  $Ha = 0$  and  $N_r = N_t = N_b = 0.1$**

Grid size	$Nu_{avg}$	$\Delta = \frac{ Nu_{i \times j} - Nu_{180 \times 180} }{Nu_{180 \times 180}} \times 100\%$
$30 \times 30$	9.823	4.5
$60 \times 60$	10.015	2.63
$90 \times 90$	10.112	1.69
$120 \times 120$	10.190	0.93
$180 \times 180$	10.286	-

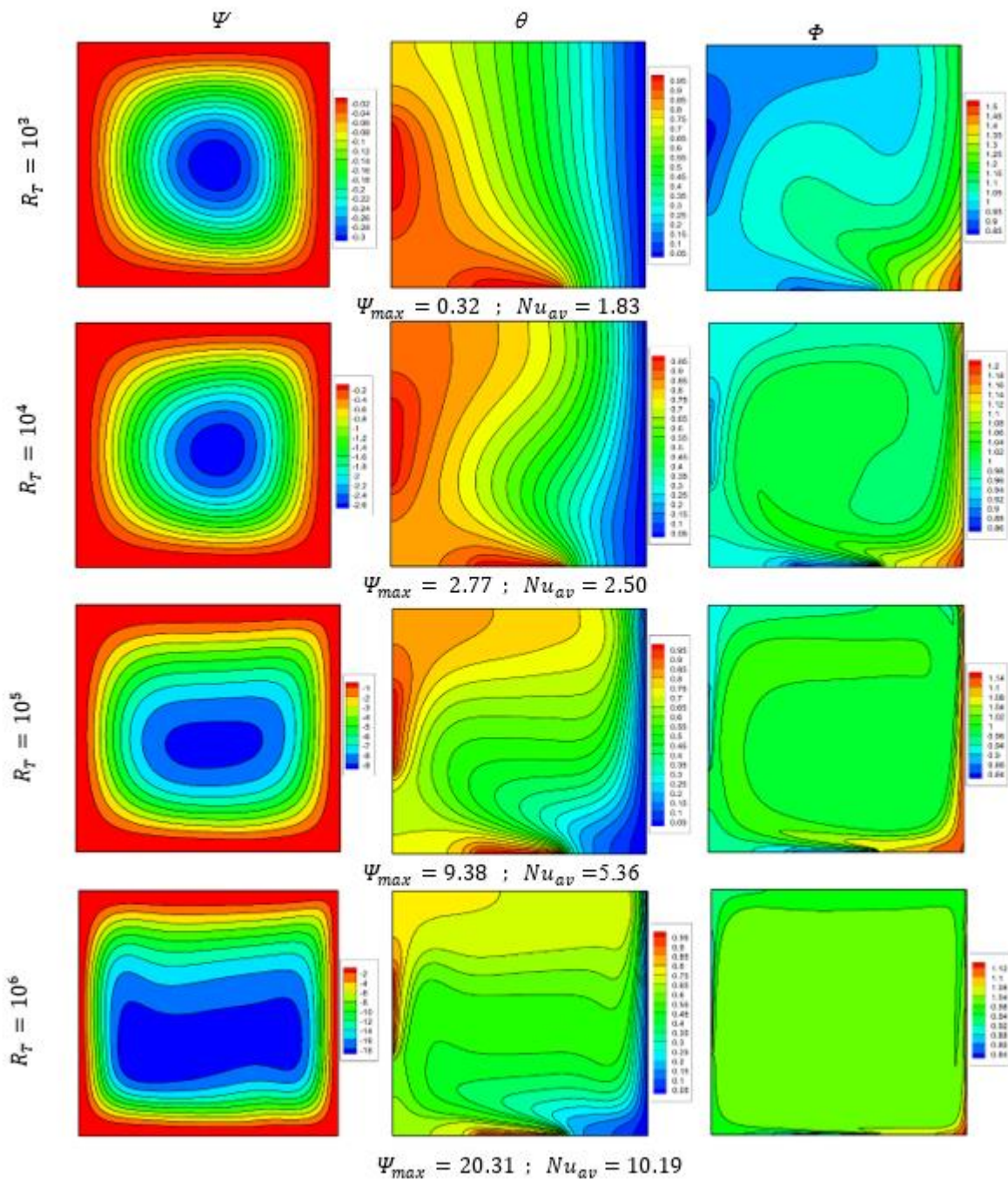


Fig. 4 Streamlines, isotherms and iso-concentrations for  $Ha = 0$ ,  $Da = 10^{-2}$ ,  $N_r = N_t = N_b = 0.1$  and various  $R_T$

#### 4. FINDINGS

This study explores natural convection in a partially heated square porous cavity filled with a nanofluid, considering the effects of a magnetic field. The findings are illustrated through streamlines, isotherms, iso-concentrations, and average Nusselt and Sherwood numbers for various  $Da$ ,  $Ha$ ,  $R_T$ ,  $N_t$ ,  $N_b$ , and  $N_r$ . The Lewis and Prandtl numbers are considered constant ( $Le = 25$  and  $Pr = 7$ ).

##### 4.1 Impact of Rayleigh Number

Figure 4 illustrates the influence of the Rayleigh

number on streamlines, isotherms and iso-concentrations without a magnetic field ( $Ha = 0$ ) for  $Da = 10^{-2}$ ,  $N_t = N_b = N_r = 0.1$  and different Rayleigh number values ( $10^3 \leq R_T \leq 10^6$ ). A single clockwise flow cell is present in the cavity, created by the upward/(downward) motion of the fluid that is heated/(cooled) by the vertical heater/(right cold wall). At low Rayleigh numbers, as shown in Fig. 4 for  $R_T = 10^3$ , the flow intensity is weak. Consequently, the isotherms are almost vertical in regions away from the heating segments, indicating that conduction primarily governs heat transfer. As the Rayleigh number rises, the flow intensity also increases, resulting in the development of boundary layers adjacent

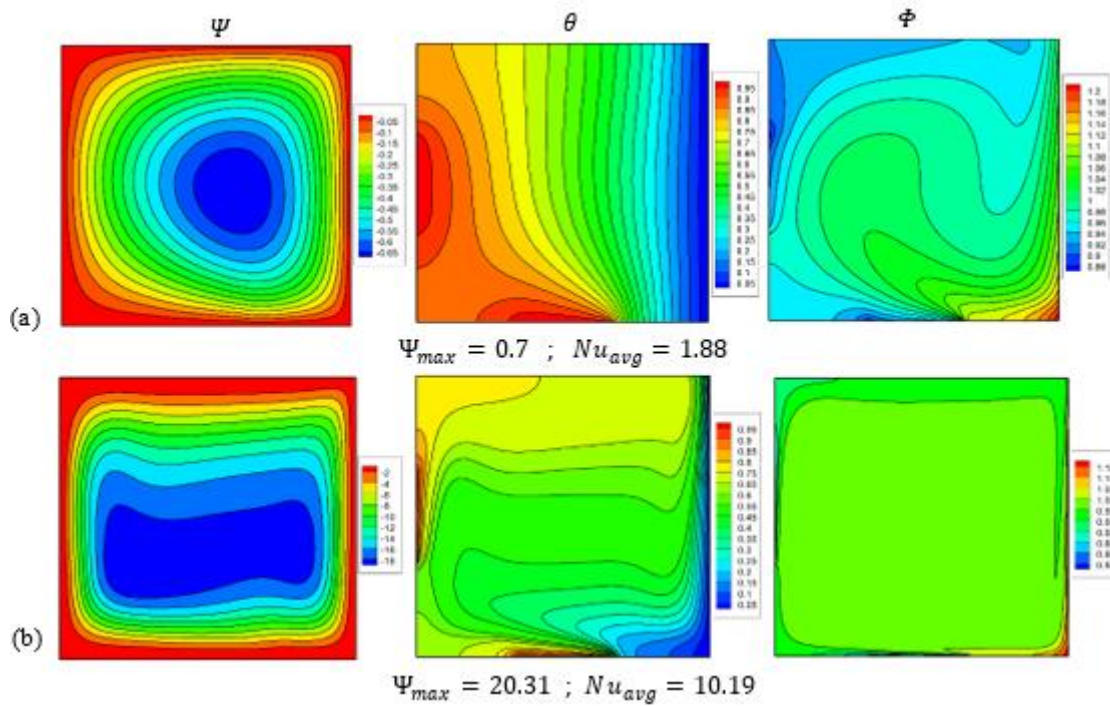


**Fig. 5** Streamlines, isotherms and isoconcentrations for  $R_T = 10^6$ ,  $Ha = 0$ ,  $N_r = N_t = N_b = 0.1$  and  $Da = 10^{-5}$  (a) and  $10^{-2}$  (b)

to the active walls at high Rayleigh numbers, such as  $R_T = 10^6$  as illustrated in Fig. 4. Quantitatively,  $\Psi_{max}$  increases from 0.32 to 20.31 as  $R_T$  rises from  $10^3$  to  $10^6$ . The isotherm pattern is significantly altered by convection effects, leading to the emergence of a vertical thermal stratification in a substantial portion of the cavity. Additionally, an increase in  $R_T$ , leads to a more uniform distribution of nanoparticles within the core of the cavity. The concentration of nanoparticles is notably higher near the cold wall, as illustrated by the iso-concentrations in Fig. 4. This phenomenon can be attributed to the thermophoresis effect, which drives higher or lighter molecules towards warmer or cooler areas, respectively.

**4.2 Effect of Darcy Number**

Figure 5 illustrates the streamlines, isotherms and isoconcentrations for the parameters  $R_T = 10^6$ ,  $Ha = 0$ ,  $N_t = N_b = N_r = 0.1$ , considering two different values of the Darcy number ( $Da = 10^{-5}$  and  $Da = 10^{-2}$ ). At a  $Da$  value of  $10^{-5}$  (see Fig. 5a), the flow intensity is relatively low ( $\Psi_{max} = 0.7$ ). Consequently, conduction effects predominantly influence the temperature field, leading to a distinctly uneven distribution of nanoparticles (refer to Fig. 5a). Increasing the Darcy number to  $Da = 10^{-2}$  markedly improves the permeability of the porous matrix, thereby promoting vigorous flow circulation within the cavity. This enhancement is evidenced by a maximum flow rate of  $\Psi_{max} = 20.31$  at this Darcy number. The structure of isotherms and iso-concentrations (refer to Fig. 5b) clearly demonstrate that convection effects primarily govern heat and mass transfer. This is supported by the formation of boundary layers and the uniform distribution of nanoparticles. Figure 6 shows the influence of the Darcy number on the dimensionless vertical velocity at the mid-height of the cavity for  $R_T = 10^6$ . This figure shows

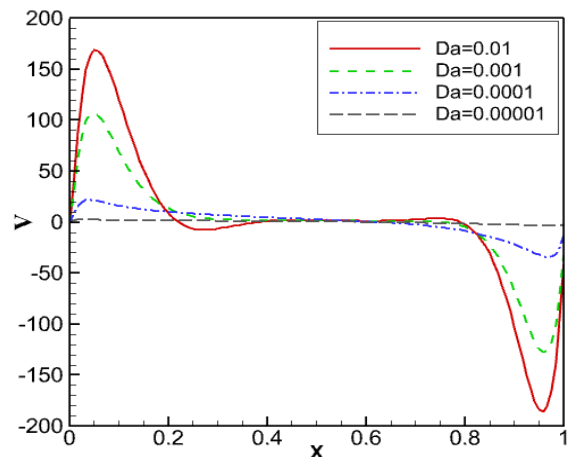


**Fig. 6** Vertical velocity profiles at mid-height of the cavity for  $R_T = 10^6$ ,  $Ha = 0$ ,  $N_r = N_t = N_b = 0.1$  and various  $Da$

that a decrease in the Darcy number results in reduced permeability of the porous matrix. Consequently, this reduction dampens the flow and suppresses the behaviour of the boundary layer.

**4.3 Effect of Hartmann number**

The impact of the Hartmann number ( $Ha$ ) on the flow, temperature, and concentration fields is illustrated in Fig. 7 for  $R_T = 10^6$ ,  $N_t = N_b = N_r = 0.1$  and  $Da = 10^{-2}$ . An increase in the magnetic field strength leads to a reduction in flow intensity and alters the trajectories of particles in the central region of the flow cell, as evidenced by the shapes of the internal streamlines. The flow intensity decreases significantly as the Hartmann number increases from 0 to 100, with  $\Psi_{max}$  dropping from 20.31 to 7.97.

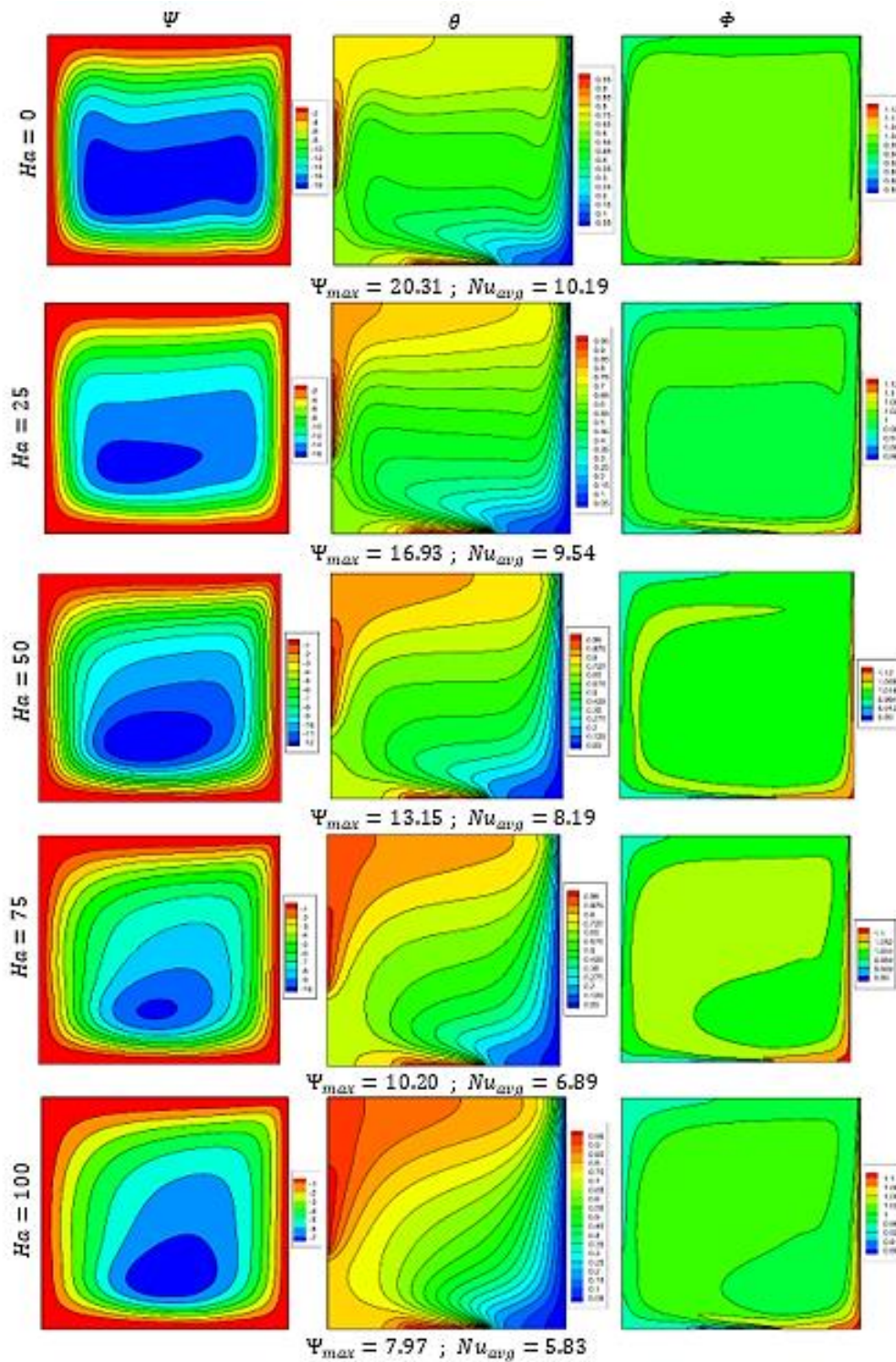


**Fig. 7** Streamlines, isotherms and isoconcentrations for  $R_T = 10^6$ ,  $Da = 10^{-2}$ ,  $N_r = N_t = N_b = 0.1$  and various  $Ha$

The damping effect of the magnetic field clearly shows the reduced flow intensity in the mid-height velocity profiles of the enclosure. (see Fig. 8a). At  $Ha = 100$ , the peak velocity is observed to be less than one-fifth of that at  $Ha = 0$ . The rise in  $Ha$  reduces convection effects and tends to eradicate the vertical thermal stratification seen in the central region of the cavity at  $Ha = 0$ , with this stratification vanishing entirely at  $Ha = 100$ . It also reduces the temperature gradient near the vertical heater and the cold wall, as illustrated by the temperature profiles

in Fig. 8b. This figure demonstrates that the magnetic field at  $Ha = 100$  disrupts the thermal boundary layer. The impact of  $Ha$  on the distribution of nanoparticles is relatively minor. As  $Ha$  increases, there is a gradual shift towards a non-homogeneous medium.

### 4.3 Influence of Thermophoresis and Brownian motion

Figure 9 depicts the influence of the parameter  $N_t$  on the streamlines, isotherms, and iso-concentrations when

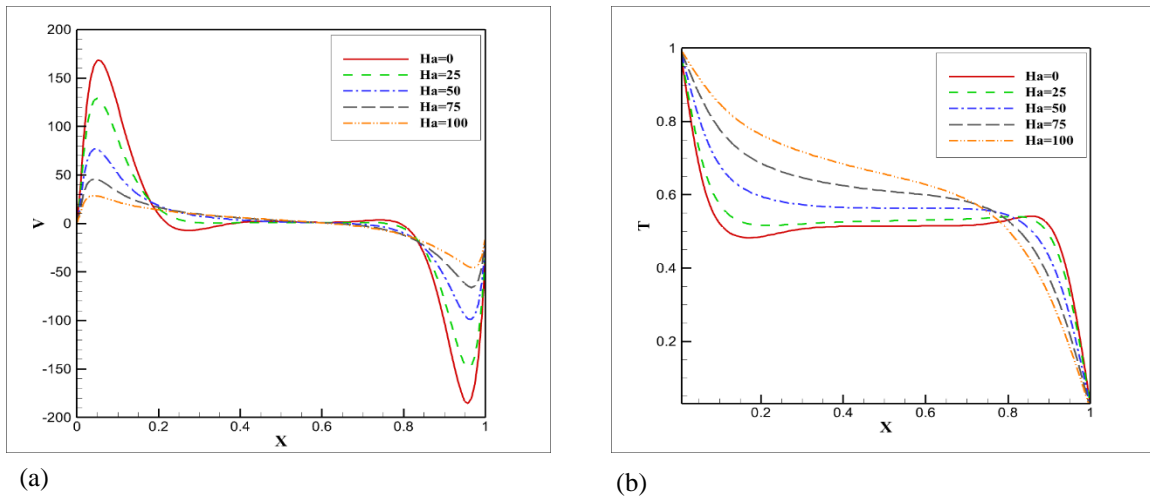


**Fig. 8** Vertical velocity profiles (a) and temperature profiles (b) at mid-height of the enclosure for  $R_T = 10^6$ ,  $Da = 10^{-2}$ ,  $N_r = N_t = N_b = 0.1$  and various  $Ha$

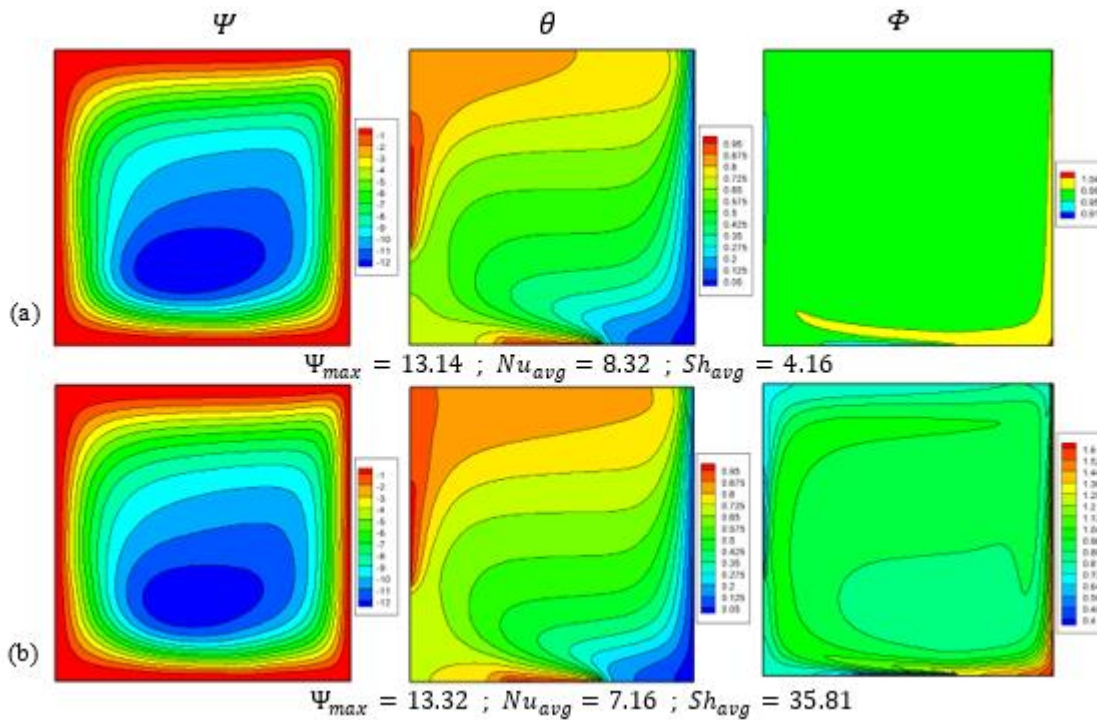


**Fig. 9** Streamlines, isotherms and iso-concentrations for  $R_T = 10^6$ ,  $Ha = 50$ ,  $Da = 10^{-2}$ ,  $N_b = N_r = 0.1$ ,  $N_t = 0.05$  (a) and  $N_t = 0.5$  (b)

$R_T = 10^6$ ,  $Da = 10^{-2}$ ,  $Ha = 50$  and  $N_r = N_b = 0.1$ . An increase in  $N_t$  has a negligible effect on the streamlines and results in a subtle alteration of the temperature field, particularly near the hot and cold walls. Here, the isotherms become somewhat less dense, suggesting a slight decrease in thermal gradients. Nevertheless, an increase in this latter parameter significantly impacts the concentration field within the enclosure. It disrupts the uniform distribution of nanoparticles seen at lower values of  $N_t$ , resulting in notable concentration gradients within the mixture.

Figure 10 illustrates the impact of the parameter  $N_b$  on streamlines, isotherms and isoconcentrations at  $R_T = 10^6$ ,  $Da = 10^{-2}$ ,  $Ha = 50$  and  $N_r = N_t = 0.1$ . The figure

indicates that an increase in  $N_b$  promotes a more uniform distribution of nanoparticles, resulting in decreased concentration gradients. However, it has minimal influence on the streamlines and isotherms.

#### 4.4 Thermal Transfer

Figure 11 illustrates how the Rayleigh number influences the average Nusselt number,  $Nu_{avg}$ , under the conditions of  $Ha = 0$ ,  $N_t = N_b = N_r = 0.1$  and different Darcy numbers. The figure clearly indicates that  $Nu_{avg}$  rises with increasing the Rayleigh number within a specific range of  $R_T$ , where convective transfer plays a significant role. When  $R_T$  falls below this range, conduction becomes the primary mode of heat transfer,

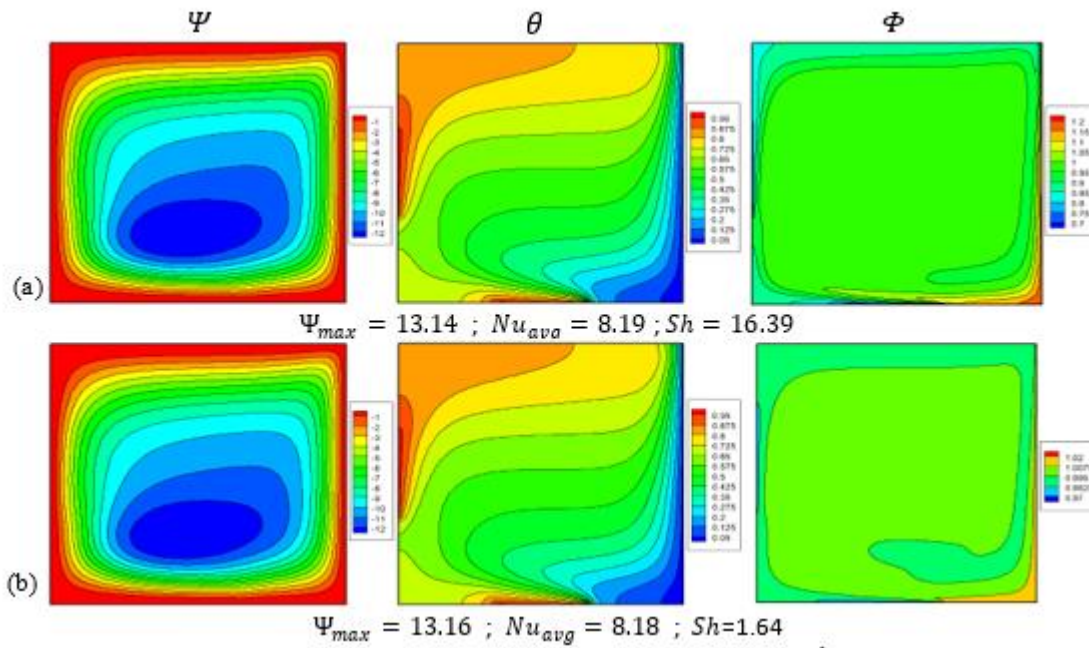


Fig. 10 Streamlines, isotherms and iso-concentrations for  $R_T = 10^6$ ,  $Ha = 50$ ,  $Da = 10^{-2}$ ,  $N_r = N_t = 0.1$ ,  $N_b = 0.05$  (a) and  $N_b = 0.5$  (b)

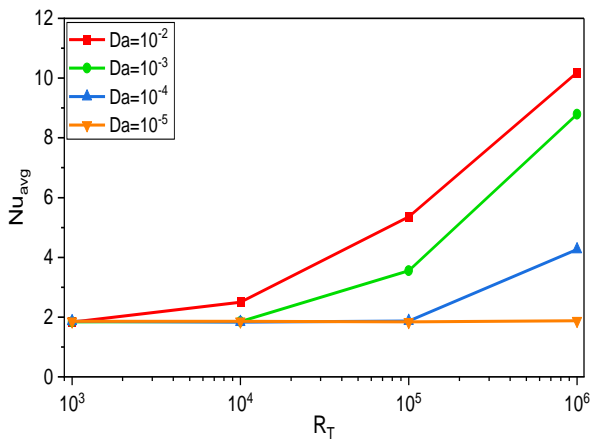
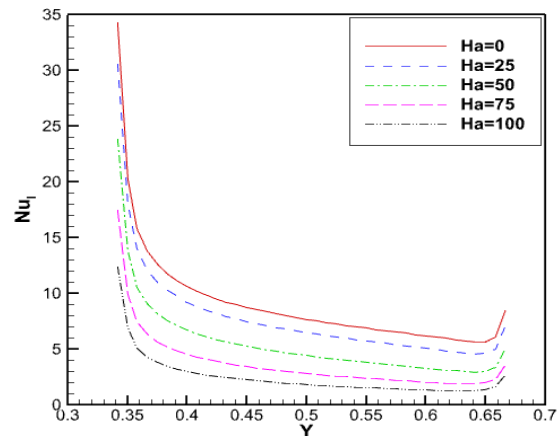


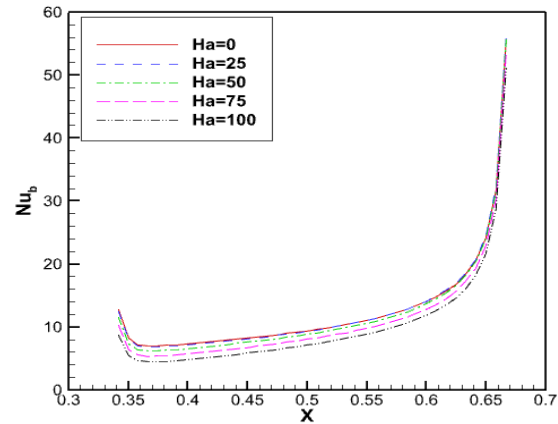
Fig. 11 Average Nusselt number vs.  $R_T$  for different Darcy number values,  $Ha = 0$  and  $N_r = N_b = N_t = 0.1$

and  $Nu_{avg}$  shows minimal sensitivity to the variations of  $R_T$ . The onset of convection is increasingly postponed as the Darcy number decreases. Specifically, for a Darcy number of  $10^{-2}$ ,  $Nu_{avg}$  increases by factors of 1.4, 2.9 and 5.6 when  $R_T$  is increased from  $10^3$  to  $10^4$ ,  $10^5$  and  $10^6$ , respectively. Increasing the Darcy number increases heat transfer efficiency. For instance, at  $R_T = 10^6$ ,  $Nu_{avg}$  decreases by approximately 13.7%, 58.13% and 81.58% as  $Da$  goes from  $10^{-2}$  to  $10^{-3}$ ,  $10^{-4}$  and  $10^{-5}$ , respectively. At higher permeability, the increased Darcy number reduces the solid matrix's resistance to flow. This reduction in resistance promotes the role of convection.

Figure 12 illustrates the variations of the local Nusselt number for the left (a) and bottom (b) hot walls, under conditions where  $R_T = 10^6$ ,  $Da = 10^{-2}$ ,  $N_t = N_b = N_r = 0.1$ , with different Hartmann numbers. The results



(a)



(b)

Fig. 12 Local Nusselt number on the left (a) and bottom (b) hot walls at  $R_T = 10^6$ ,  $Da = 10^{-2}$ ,  $N_r = N_b = N_t = 0.1$  and different  $Ha$

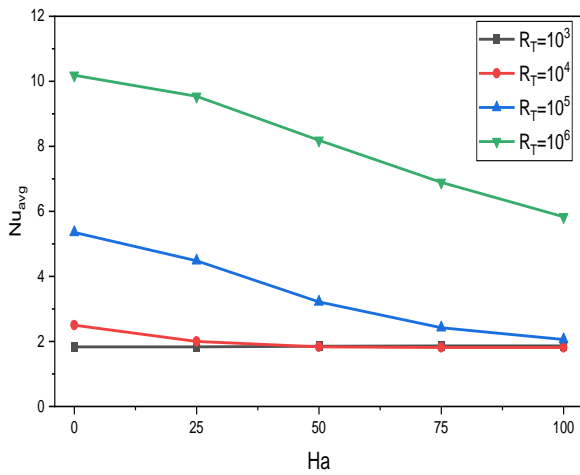
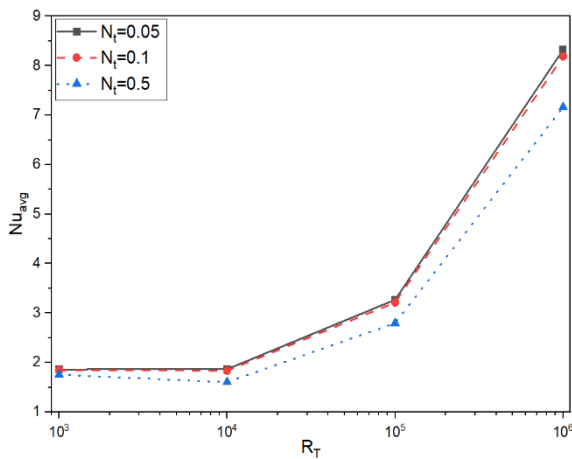
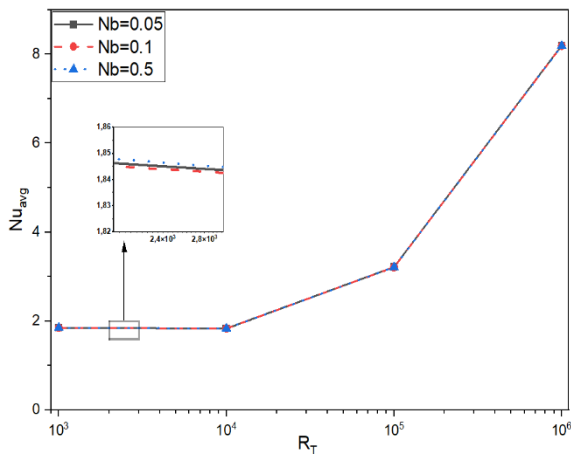


**Fig. 13** Average Nusselt number vs.  $Ha$  for  $Da = 10^{-2}$ ,  $N_r = N_b = N_t = 0.1$  and various  $R_T$



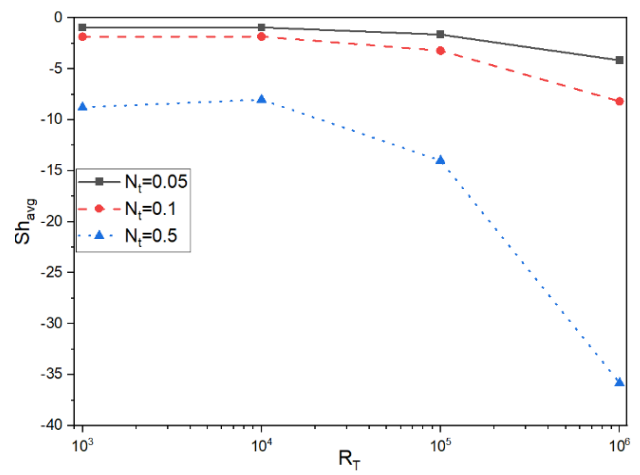
(a)



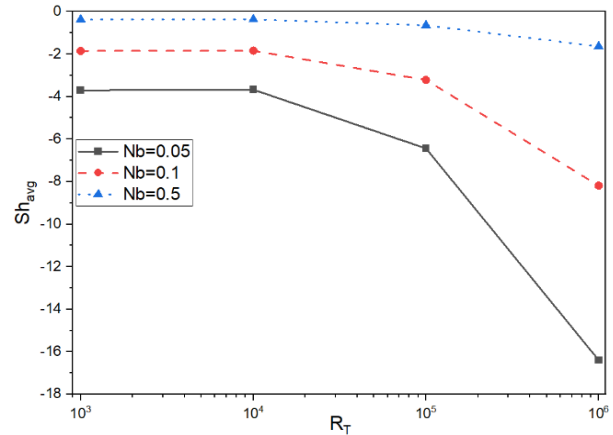
(b)

**Fig. 14** Average Nusselt number vs.  $R_T$  for  $Da = 10^{-2}$ ,  $Ha = 50$ ,  $N_r = 0.1$  and different values of thermophoresis (a) and Brownian parameters (b)

show that increasing the magnetic field strength decreases the local Nusselt number on the heated walls, particularly on the left hot wall, as seen in Figs. 7, indicating significant flow attenuation in that region.



(a)



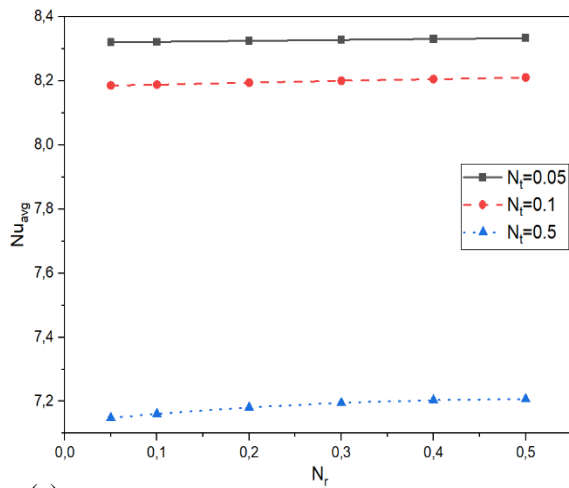
(b)

**Fig. 15** Average Sherwood number vs.  $R_T$  for  $Da = 10^{-2}$ ,  $Ha = 50$ ,  $N_r = 0.1$  and different values of thermophoresis (a) and Brownian parameters (b)

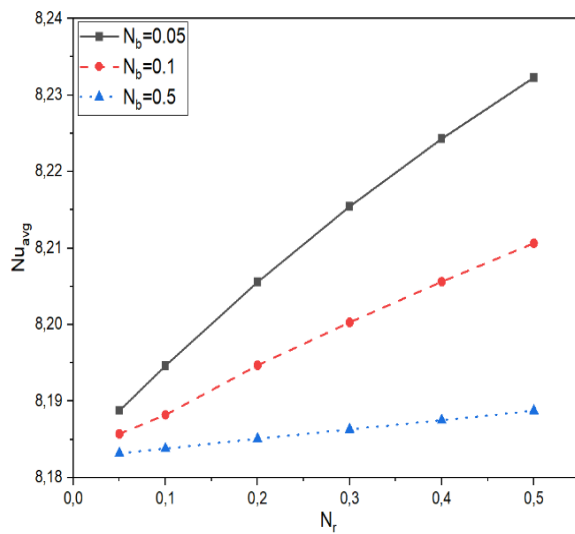
Figure 13 illustrates the influence of  $Ha$  on the average Nusselt number for a Darcy number of  $10^{-2}$ , with  $N_r = N_b = N_t = 0.1$  and varying values of  $R_T$ . The figure demonstrates that  $R_T$  and  $Ha$  exert opposing effects on  $Nu_{avg}$ . Specifically, an increase in  $R_T/(Ha)$  leads to an enhancement/(a reduction) in heat transfer.

When  $R_T = 10^3$ , the average Nusselt number remains almost constant ( $Nu_{avg} = 1.83$ ), indicating dominance by conduction. Conversely, for values of  $R_T$  ranging from  $10^4$  to  $10^6$ , convection effects become significant but they are attenuated by increasing the Hartmann number. Quantitatively, as the Hartmann number increases from 0 (indicating the absence of a magnetic field) to 100,  $Nu_{avg}$  drops by 27.25%, 61.48% and 42.76% for  $R_T = 10^4$ ,  $R_T = 10^5$  and  $R_T = 10^6$ , respectively. This data suggests that the most significant effect of  $Ha$  on heat transfer occurs at  $R_T = 10^5$ .

Figures 14a and 14b depict the variations of the mean Nusselt number ( $Nu_{avg}$ ) vs.  $R_T$  for various values of the thermophoresis parameter,  $N_t$ , and the Brownian parameter,  $N_b$ , respectively.



(a)



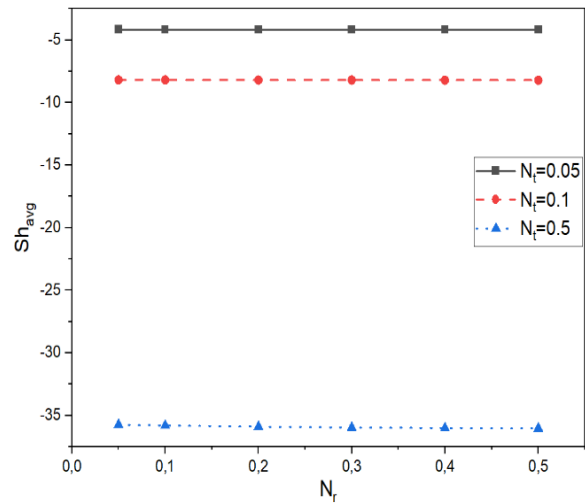
(b)

**Fig. 16 Average Nusselt number vs. buoyancy ratio parameter for various  $N_t$  (a) and  $N_b$  (b)**

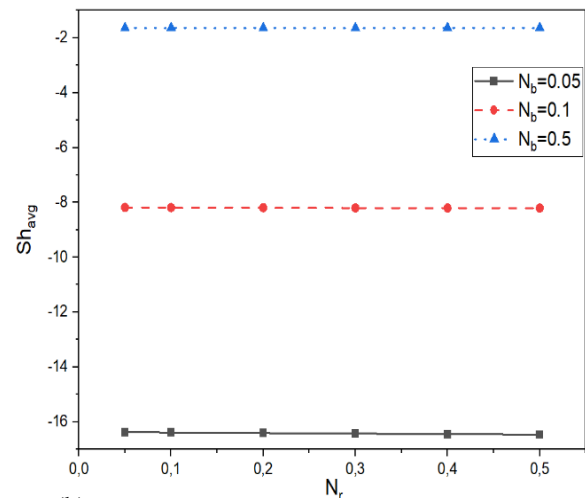
Notably, an increase in  $N_t$  results in a significant decrease in  $Nu_{avg}$ . For instance, at  $R_T = 10^5$ ,  $Nu_{avg}$  decreases by 14.5% when  $N_t$  is increased from 0.05 to 0.5. In contrast, variations in  $N_b$  produce minimal changes in  $Nu_{avg}$ , as illustrated in Fig. 14(b).

The average Sherwood number ( $Sh_{avg}$ ) variations versus  $R_T$  for different values of  $N_t$  and  $N_b$  are illustrated in Figs 15a and 15b, respectively. Remarkably, an increase in  $N_t$  results in a significant increase in the absolute value of  $Sh_{avg}$ , as depicted in Fig. 15(a). For instance, at  $R_T = 10^6$ , the absolute value of  $Sh_{avg}$  increases by a factor of 8.6 when  $N_t$  rises from 0.05 to 0.5. Additionally, the increase in  $N_b$  significantly impacts  $Sh_{avg}$  (see Fig. 15(b)). Hence, at  $R_T = 10^6$ ,  $|Sh_{avg}|$  decreases by a factor of 10 as  $N_b$  changes from 0.05 to 0.5.

Figure 16 illustrates the influence of  $N_r$  on the Nusselt number for  $N_b = 0.1/(N_t = 0.1)$  and various  $N_t/(N_b)$  at  $R_T = 10^6$ ,  $Da = 10^{-2}$  and  $Ha = 50$ . The results indicate



(a)



(b)

**Fig. 17 Average Sherwood number vs. buoyancy ratio parameter for various  $N_t$  (a) and  $N_b$  (b)**

$R_T = 10^6$ ,  $Da = 10^{-2}$  and  $Ha = 50$ . The results indicate that  $Nu_{avg}$  shows minimal sensitivity to changes in  $N_r$  variations for  $N_t$  values of 0.05 and 0.1. However, for  $N_t = 0.5$ , there is a gradual increase in  $Nu_{avg}$  as  $N_r$  varies, as depicted in Fig. 16(a).

Figure 16(b) illustrates that the impact of  $N_r$  on  $Nu_{avg}$  is more pronounced at lower values of  $N_b$ . However, even at the smallest value of  $N_b$  value examined in this study ( $N_b = 0.05$ ), the increase in  $Nu_{avg}$  when  $N_r$  is increased from 0.05 to 0.5 is less than 0.6%.

The graphs depicting the average Sherwood number variations versus  $N_r$  (Figure 17) indicate that the influence of the buoyancy ratio on mass transfer is negligible within the range of parameters analysed.

## 5. CONCLUSION

This study investigates magnetohydrodynamic (MHD) natural convection within a square porous enclosure filled with a nanofluid. The enclosure is heated from the bottom

and left walls and cooled from the right side. The analysis employs Buongiorno's model and utilises a computational code developed on the finite volume method, incorporating the SIMPLE algorithm to solve the governing equations. Comprehensive validation processes were carried out through comparisons with established results. The comparison produced very promising results, within an error margin under 1.5%, which confirms the accuracy and reliability of our simulations.

In scenario where the magnetic field is absent ( $Ha = 0$ ), it is observed that an increase in the Rayleigh/Darcy number has a significant impact on the flow, temperature, and concentration fields. This results in enhanced flow intensity and improved convective heat transfer, while simultaneously decreasing the non-homogeneity of nanoparticles distribution in the medium.

When a magnetic field is present ( $Ha \neq 0$ ), the primary conclusions of this research are:

Increasing the Hartmann number diminishes convection effects and reduces the vertical thermal stratification seen in the cavity's center at  $Ha = 0$ . Additionally, it attenuates the temperature gradients near the vertical active walls.

The magnetic field at  $Ha = 100$  disrupts the thermal boundary layer.

The impact of  $Ha$  on the distribution of nanoparticles is minimal. It shows a gradual shift towards a non-homogeneous medium as  $Ha$  increases.

The rise in  $N_t$  results in a reduction/(an enhancement) of  $Nu_{avg}/(|Sh_{avg}|)$ .

The increase in  $N_b$  leads to a reduction in  $|Sh_{avg}|$ , but has little to no impact on  $Nu_{avg}$ .

The impact of  $N_r$  on both  $Nu_{avg}$  and  $Sh_{avg}$  is negligible under the considered conditions.

## CONFLICT OF INTEREST

The authors have no conflicts to disclose.

## AUTHORS CONTRIBUTION

**A. Marfouk** and **A. Mansour** performed numerical simulation, project investigation and validation. They also wrote the manuscript. **A. Hasnaoui**, **A. Amahmid** and **M. Hasnaoui** examined the manuscript and supervised all the work of the article

## REFERENCES

Ahmed, S. E., Mansour, M. A., Rashad, A. M., & Salah, T. (2020). MHD natural convection from two heating modes in finned triangular enclosures filled with porous media using nanofluids. *Journal of Thermal Analysis and Calorimetry*, 139(5), 3133-3149. <https://doi.org/10.1007/s10973-019-08675-x>

Alsabery, A. I., Saleh, H., Hashim, I., & Hussain, S. H. (2016). Darcian natural convection in inclined square cavity partially filled between the central square hole filled with a fluid and inside a square porous cavity filled with nanofluid. *Journal of Applied Fluid Mechanics*, 9(4), 1763-1775. <https://doi.org/10.18869/acadpub.jafm.68.235.24575>

Alsabery, A. I., Sheremet, M. A., & Chamkha, A. J. (2018). Conjugate natural convection of Al<sub>2</sub>O<sub>3</sub>-water nanofluid in a square cavity with a concentric solid insert using Buongiorno's two-phase model. *International Journal of Mechanical Sciences*, 136, 200-219. <https://doi.org/10.1016/j.ijmecsci.2017.12.025>

Babar, H., & Ali, H. M. (2019). Airfoil shaped pin-fin heat sink: potential evaluation of ferric oxide and titania nanofluids. *Energy Conversion and Management*, 202, 112194. <https://doi.org/10.1016/j.enconman.2019.112194>

Benygzer, C., Bouzit, M., Mokhefi, A., & Khelif, F. (2022). Unsteady natural convection in a porous square cavity saturated by nanofluid using buongiorno model: variable permeability effect on homogeneous porous medium. *CFD Letters*, 14(7), 42-61. <https://doi.org/10.37934/cfdl.14.7.4261>

Bondareva, N. S., Sheremet, M. A., Oztop, H. F., & Abu-Hamdeh, N. (2017). Entropy generation due to natural convection of a nanofluid in a partially open triangular cavity. *Advanced Powder Technology*, 28, 244-255. <https://doi.org/10.1016/j.apt.2016.09.030>

Bondareva, N. S., Sheremet, M. A., Oztop, H. F., & Abu-Hamdeh, N. (2016). Heatline visualization of MHD natural convection in an inclined wavy open porous cavity filled with a nanofluid with a local heater. *International Journal of Heat and Mass Transfer*; 99, 872-881. <https://doi.org/10.1016/j.ijheatmasstransfer.2016.04.055>

Buongiorno, J. (2006). Convective transport in nanofluids. *ASME Journal of Heat Transfer*, 128(3), 240-250. <https://doi.org/10.1115/1.2150834>

Calcagni B., Marsili F., & Paroncini M. (2005). Natural convective heat transfer in square enclosures heated from below. *Applied Thermal Engineering*, 25, 2522-2531. <https://doi.org/10.1016/j.applthermaleng.2004.11.032>

Choi, S. U. S., & Eastman, J. A. (1995, November 12-17). *Enhancing thermal conductivity of fluids with nanoparticles*. ASME International Mechanical Engineering Congress & Exposition, San Francisco, United States: N. p., 1995.

Jafari, Y., Taeibi-Rahni, M., Haghshenas, M., & Ramian, P. (2018). Lattice boltzmann numerical investigation of inner cylindrical pin-fins configuration on nanofluid natural convective heat transfer in porous enclosure. *Journal of Applied Fluid Mechanics*, 11

- (3), 801-816. <https://doi.org/10.29252/jafm.11.03.27945>
- Kahveci, K. (2010). Buoyancy driven heat transfer of nanofluids in a tilted enclosure. *Journal of Heat Transfer*; 132(6) 062501. (12 pages). <https://doi.org/10.1115/1.4000744>
- Kasaeian, A., Daneshzarian, R., Mahian, O., Kolsi, L., Chamkha, A. J., Wongwises, S., & Pop, I. (2017). Nanofluid flow and heat transfer in porous media: a review of the latest developments. *International Journal of Heat and Mass Transfer*, 107, 778-791. <https://doi.org/10.1016/j.ijheatmasstransfer.2016.11.074>
- Kefayati, G. R. (2014). Effect of a magnetic field on natural convection in a nanofluid-filled enclosure with a linearly heated wall using LBM. *Arabian Journal for Science and Engineering*, 39, 4151-4163. <https://doi.org/10.1007/s13369-014-1031-9>
- Khanafer, K., & Vafai, K. (2019). Applications of nanofluids in porous medium. *Journal of Thermal Analysis and Calorimetry*, 135, 1479-1492. <https://doi.org/10.1007/s10973-018-7565-4>
- Li, S., Abbasi, A., Farooq, W., Gul, M., Khan, M.I., Nafasova, G., & Hejazi, H. A., (2024a). Heat and mass transfer characteristics of Al<sub>2</sub>O<sub>3</sub>/H<sub>2</sub>O and (Al<sub>2</sub>O<sub>3</sub>+ Ag)/H<sub>2</sub>O nanofluids adjacent to a solid sphere: A theoretical study. *Numer. Heat trans. Part A: applications*. 1-19. <https://doi.org/10.1080/10407782.2024.2306177>
- Li, S., Khan, M.I., Ali, S., Ullah Khan, S., Althobaiti, S.A., Khan, I., & Kchaou, M., (2024b). Influence of variable fluid properties on mixed convective Darcy–Forchheimer flow relation over a surface with Soret and Dufour spectacle. *Open Physics* 22(1) 20240010. <https://doi.org/10.1515/phys-2024-0010>
- McNab, G. S., & Meisen, A. (1973). Thermophoresis in liquids. *Journal of Colloid and Interface Science*, 44 (2), 339-346. [https://doi.org/10.1016/0021-9797\(73\)90225-7](https://doi.org/10.1016/0021-9797(73)90225-7).
- Motlagh, S. Y., Taghizadeh, S., & Soltanipour, H. (2016). Natural convection heat transfer in an inclined square enclosure filled with a porous medium saturated by nanofluid using Buongiorno's mathematical model. *Advanced Powder Technology*, 27(6), 2526-2540. <https://doi.org/10.1016/j.appt.2016.09.016>
- Narla, V. K., Tripathi, D., & Bég, O. A. (2020). Analysis of entropy generation in biomimetic electroosmotic nanofluid pumping through a curved channel with joule dissipation. *Thermal Science and Engineering Progress*, 15. <https://doi.org/10.1016/j.tsep.2019.100424>.
- Nazari, M. A., Ghasempour, R., & Ahmadi, M. H. (2019). A review on using nanofluids in heat pipes. *Journal of Thermal Analysis and Calorimetry*, 137, 1847-1855. <https://doi.org/10.1007/s10973-019-08094-y>
- Oztop, H. F., & Abu-Nada, E. (2008). Numerical study of natural convection in partially heated rectangular enclosures filled with nanofluids. *International Journal of Heat and Fluid Flow*, 29(5), 1326-1336. <https://doi.org/10.1016/j.ijheatfluidflow.2008.04.009>
- Patankar, S. V. (1980). *Numerical heat transfer and fluid flow*. Hemisphere Publishing Corporation. Taylor and Francis Group, New York, 113-137.
- Prakash, J., Sharma, A. & Tripathi, D. (2020). Convective heat transfer and double diffusive convection in ionic nanofluids flow driven by peristalsis and electromagnetohydrodynamics. *Pramana – Journal of Physics*, 94(4). <https://doi.org/10.1007/s12043-019-1873-5>
- Prakash, J., Siva, E. P., Tripathi, D., & Bég, O. A. (2019a). Thermal slip and radiative heat transfer effects on electro-osmotic magneto nanoliquid peristaltic propulsion through a microchannel. *Heat Transfer Asian Research*, 48(7), 2882-2908. <https://doi.org/10.1002/htj.21522>
- Prakash, J., Siva, E. P., Tripathi, D., Kuharat, S., & Bég, O. A. (2019b). Peristaltic pumping of magnetic nanofluids with thermal radiation and temperature-dependent viscosity effects: modelling a solar magneto biomimetic nanopump. *Renewable Energy*, 133, 1308-13026. <https://doi.org/10.1016/j.renene.2018.08.096>
- Rahimi, A., Dehghan Saeed, A., Kasaeipoor, A., & Hasani Malekshah, E. (2019). A comprehensive review on natural convection flow and heat transfer: the most practical geometries for engineering applications. *International Journal of Numerical Methods for Heat & Fluid Flow*, 29(3), 834-877. <https://doi.org/10.1108/HFF-06-2018-0272>
- Sajid, M. U., Ali, H. M., Sufyan, A., Rashid, D., Zahid, S. U., & Rehman, W. U. (2019). Experimental investigation of TiO<sub>2</sub>-water nanofluid flow and heat transfer inside wavy mini-channel heat sinks. *Journal of Thermal Analysis and Calorimetry*, 137(4), 1279-1294. <https://doi.org/10.1007/s10973-019-08043-9>
- Sammoud, M., & Gueraoui, K. (2021). MHD double diffusive convection of Al<sub>2</sub>O<sub>3</sub>-water nanofluid in a porous medium filled an annular space inside two vertical concentric cylinders with discrete heat flux. *Journal of Applied Fluid Mechanics*, 14(5), 1459-1468. <https://doi.org/10.47176/jafm.14.05.32388>
- Sheikholeslami, M. (2018a). Magnetic source impact on nanofluid heat transfer using CVFEM. *Neural Computing and Applications*, 30, 1055-1064. <https://doi.org/10.1007/s00521-016-2740-7>
- Sheikholeslami, M. (2018b). New computational approach for exergy and entropy analysis of nanofluid under the impact of Lorentz force through a porous media, *Comput. Methods in Applied Mechanics and Engineering*, 344, 319-333. <https://doi.org/10.1016/j.cma.2018.09.044>
- Sheikholeslami, M. (2019). Numerical approach for MHD Al<sub>2</sub>O<sub>3</sub>-water nanofluid transportation inside a

- permeable medium using innovative computer method, *Comput. Computer Methods in Applied Mechanics and Engineering* 344, 306–318. <https://doi.org/10.1016/j.cma.2018.09.042>
- Sheikholeslami, M., & Shehzad, S. A. (2017). RETRACTED: Magnetohydrodynamic nanofluid convective flow in a porous enclosure by means of LBM. *International Journal of Heat and Mass Transfer*, 113, 796-805. <https://doi.org/10.1016/j.ijheatmasstransfer.2017.05.130>
- Sheikholeslami, M., & Ellahi R. (2015). Three dimensional mesoscopic simulation of magnetic field effect on natural convection of nanofluid. *International Journal of Heat and Mass Transfer*, 89, 799-808. <https://doi.org/10.1016/j.ijheatmasstransfer.2015.05.110>
- Sheremet, M. A., Groşan, T., & Pop, I. (2014). Free convection in shallow and slender porous cavities filled by a nanofluid using buongiorno's model. *ASME. Journal of Heat Transfer*, 136(8), 082501. <https://doi.org/10.1115/1.4027355>
- Sheremet, M. A., Grosan, T., & Pop, I. (2015). Steady-state free convection in right-angle porous trapezoidal cavity filled by a nanofluid: Buongiorno's mathematical model. *European Journal of Mechanics - B/Fluids*, (53), 241-250. <https://doi.org/10.1016/j.euromechflu.2015.06.003>
- Zahmatkesh, I., & Habibi, M. R. (2019). Natural and mixed convection of a nanofluid in porous cavities: critical analysis using buongiorno's model. *Journal of Theoretical and Applied Mechanics*, 57(1), 221-233. <https://doi.org/10.15632/jtam-pl.57.1.221>